



**HAL**  
open science

# Catalytic Fast Pyrolysis of Biomass over Microporous and Hierarchical Zeolites: Characterization of Heavy Products

Jasmine Hertzog, Vincent Carré, Liangyuan Jia, Colin Logan Mackay, Ludovic Pinard, Anthony Dufour, Ondřej Mašek, Frederic Aubriet

► **To cite this version:**

Jasmine Hertzog, Vincent Carré, Liangyuan Jia, Colin Logan Mackay, Ludovic Pinard, et al.. Catalytic Fast Pyrolysis of Biomass over Microporous and Hierarchical Zeolites: Characterization of Heavy Products. *ACS Sustainable Chemistry & Engineering*, 2018, 6 (4), pp.4717 - 4728. 10.1021/acssuschemeng.7b03837 . hal-01922918

**HAL Id: hal-01922918**

<https://hal.univ-lorraine.fr/hal-01922918v1>

Submitted on 14 Mar 2024

**HAL** is a multi-disciplinary open access archive for the deposit and dissemination of scientific research documents, whether they are published or not. The documents may come from teaching and research institutions in France or abroad, or from public or private research centers.

L'archive ouverte pluridisciplinaire **HAL**, est destinée au dépôt et à la diffusion de documents scientifiques de niveau recherche, publiés ou non, émanant des établissements d'enseignement et de recherche français ou étrangers, des laboratoires publics ou privés.



THE UNIVERSITY *of* EDINBURGH

Edinburgh Research Explorer

## Catalytic fast pyrolysis of biomass over microporous and hierarchical zeolites: characterization of heavy products

### Citation for published version:

Hertzog, J, Carre, V, Jia, L, Mackay, C, Pinard, L, Dufour, A, Masek, O & Aubriet, F 2018, 'Catalytic fast pyrolysis of biomass over microporous and hierarchical zeolites: characterization of heavy products', *ACS Sustainable Chemistry & Engineering*. <https://doi.org/10.1021/acssuschemeng.7b03837>

### Digital Object Identifier (DOI):

[10.1021/acssuschemeng.7b03837](https://doi.org/10.1021/acssuschemeng.7b03837)

### Link:

[Link to publication record in Edinburgh Research Explorer](#)

### Document Version:

Peer reviewed version

### Published In:

ACS Sustainable Chemistry & Engineering

### General rights

Copyright for the publications made accessible via the Edinburgh Research Explorer is retained by the author(s) and / or other copyright owners and it is a condition of accessing these publications that users recognise and abide by the legal requirements associated with these rights.

### Take down policy

The University of Edinburgh has made every reasonable effort to ensure that Edinburgh Research Explorer content complies with UK legislation. If you believe that the public display of this file breaches copyright please contact [openaccess@ed.ac.uk](mailto:openaccess@ed.ac.uk) providing details, and we will remove access to the work immediately and investigate your claim.



This document is confidential and is proprietary to the American Chemical Society and its authors. Do not copy or disclose without written permission. If you have received this item in error, notify the sender and delete all copies.

## Catalytic fast pyrolysis of biomass over microporous and hierarchical zeolites: characterization of heavy products

Journal:	<i>ACS Sustainable Chemistry &amp; Engineering</i>
Manuscript ID	sc-2017-03837z.R1
Manuscript Type:	Article
Date Submitted by the Author:	n/a
Complete List of Authors:	Hertzog, Jasmine; Université de Lorraine, LCP-A2MC - ICPM Carré, Vincent; Université de Lorraine, LCP-A2MC Jia, Liangyuan; CNRS, Reactions & Processes Engineering Laboratory (LRGP) Mackay, Colin; University of Edinburgh, Chemistry Pinard, Ludovic; Université de poitiers, LACCO Dufour, Anthony; CNRS, Reactions & Processes Engineering Laboratory (LRGP) Masek, Ondrej; University of Edinburgh School of GeoSciences, School of GeoScience Aubriet, Frédéric; Université de Lorraine, LCPMC - ICPM

SCHOLARONE™  
Manuscripts

## Catalytic fast pyrolysis of biomass over microporous and hierarchical zeolites: characterization of heavy products

Jasmine Hertzog<sup>1</sup>, Vincent Carré<sup>1</sup>, Liangyuan Jia<sup>2</sup>, Colin Logan Mackay<sup>3</sup>, Ludovic Pinard<sup>4</sup>, Anthony Dufour<sup>2</sup>, Ondřej Mašek<sup>5</sup>, Frédéric Aubriet<sup>1</sup>

- 1 LCP-A2MC, FR 2843 Institut Jean Barriol de Chimie et Physique Moléculaires et Biomoléculaires, FR 3624 Réseau National de Spectrométrie de Masse FT-ICR à très haut champ, Université de Lorraine, ICPM, 1 boulevard Arago, 57078 Metz Cedex 03, France
- 2 LRGP, CNRS, Université de Lorraine, ENSIC, 1, Rue Grandville, 54000 Nancy, France
- 3 SIRCAMS, School of Chemistry, University of Edinburgh, Edinburgh, EH9 3FJ, United Kingdom
- 4 IC2MP, 4 Rue Michel Brunet, TSA 51106, 86073 Poitiers Cedex 9, France
- 5 UK Biochar Research Center, School of Geosciences, University of Edinburgh, Kings Buildings, Edinburgh, EH9 3JN, United Kingdom

### Synopsis:

Ultra-high resolution mass spectrometry combining various ion sources demonstrates the effects of hierarchical zeolite on the heavy molecular composition of bio-oil generated by fast-pyrolysis of lignocellulosic biomass.

## ABSTRACT

The conversion of lignocellulosic biomass by catalytic fast pyrolysis (CFP) is a promising route to produce green aromatics and sustainable biofuels. The zeolite catalysts present a high ability to produce light aromatics but also heavy products. In this work, these heavy products are monitored by a well-established petroleomic approach. The selectivity towards the heavy bio-oil components of both a common HZSM-5 zeolite and a hierarchical zeolite was investigated. Part of molecular species from lignin derivatives is still present in the upgraded bio-oils. Deoxygenation and aromatization are the main modifications of the heavy compounds caused by zeolites especially for the sugarcane derivatives. These effects are stronger for the hierarchical zeolite for which numerous heavy hydrocarbons (not oxygenated) are generated due to enhanced mass transfers within the crystallites. Moreover, this catalyst demonstrates a better stability upon an increase in the biomass-to-catalyst ratio.

**Keywords:** FTICRMS, HZSM-5, bio-oil, petroleomic approach, lignocellulosic biomass, ESI, LDI, APPI

## INTRODUCTION

Fossil energies are source of critical issues dealing with ecology and economy. Their decreases while global population and energy demand increase are forcing us to develop new and greener alternatives.<sup>1</sup> Among them, bio-oil from the fast pyrolysis of lignocellulosic biomass is a promising one. As a matter of fact, this resource is renewable and bio-oils could be attractive to produce value-added chemicals and green fuels.<sup>2</sup> However, the chemical analyses performed on the bio-oil from the fast pyrolysis of lignocellulosic biomass have evidenced that this liquid was composed of thousands species and was highly oxygenated.<sup>3,4</sup> This last characteristic is responsible of high viscosity, reactivity, and corrosion, which does not allow its storage and its direct use as biofuel.<sup>5-7</sup> To overcome this hurdle, different technics are developed to upgrade bio-oils by reducing its oxygen content and increasing its energy density.<sup>8</sup> There are the physical treatments such as filtration or emulsions.<sup>9</sup> But the most common upgrading treatment is the catalysis for which two methods are explored.<sup>10,11</sup> The first one, the hydrodeoxygenation (HDO) consists in removing, or at least dramatically reducing, oxygen content in the presence of hydrogen and metal-based catalyst.<sup>9</sup> In spite of the high efficiency of the deoxygenation process, this method requires a substantial quantity of H<sub>2</sub> gas. The second method involves zeolites that are widely used for the upgrade of petroleum and can be applied to bio-oil.<sup>12,13</sup> This process is called "catalytic fast pyrolysis" (CFP). The microporous structures of zeolite present active sites, mostly acidic, where the oxygenated volatiles may undergo deoxygenation reactions. Aromatic formation is promoted but zeolite also generates coke deposit at its surface, which is responsible of its deactivation. Nevertheless, this microporous material presents many advantages such as its low cost comparing to noble metal often involved in the HDO. Moreover, different kinds of zeolite can be produced regarding its pore size and its composition. This catalyst can be directly mixed with the feedstock in the pyrolysis reactor (*in situ* catalytic fast pyrolysis). Such upgrading configuration may be less advantageous than the *ex situ* one due to ash deposit on the catalyst, which leads to a decrease of its efficiency.<sup>14</sup> To limit the deactivation of the zeolite catalyst, hierarchical zeolite catalysts are developed to enlarge the pore structure in order to increase the accessibility of reactants to the active sites.<sup>15</sup>

1  
2  
3 To assess the efficiency of such upgrading process, global data, obtained from  
4 technics such as IR spectroscopy, may be very interesting<sup>16</sup> but comprehensive molecular  
5 characterization of the bio-oil is also necessary.  
6  
7

8 While numerous studies have focused on the selectivity of the upgrading treatment  
9 on the gas and light bio-oil compounds, such as phenols and mono-aromatics, the  
10 information on the heavy ones are usually missing.<sup>17-19</sup> Moreover, numerous heavy  
11 compounds, which are primary components of bio-oils, are also paramount. They may  
12 survive or be chemically modified and/or may lead to prematurely block the treatment (by  
13 coking the catalyst for example). Consequently, achieving the most exhaustive description of  
14 these heavy compounds provides deep insight into the selectivity of the catalyst and finally  
15 leads to optimize the process parameters to produce a well-controlled refined bio-oil.<sup>11</sup> For  
16 HDO treatment, by analyzing a broader range of compounds using (-) ESI FT-ICR MS, <sup>1</sup>H NMR,  
17 and GC-MS, Bi *et al.*<sup>20</sup> highlighted compositional changes of light and heavy compounds  
18 between raw and upgraded pyrolysis oils. This non-targeted approach indicated that HDO  
19 treatment leads to a shift of oxygenated compounds to lower and narrower oxygen atom  
20 number. Similar observations were done by Koike *et al.*<sup>21</sup> who performed (-) ESI FT-ICR MS  
21 analyses to characterize raw and HDO pyrolysis bio-oils on different nickel-based catalysts.  
22 They also demonstrated that the mass range of the mass spectra achieved for the different  
23 samples was shifted to lower *m/z* values and/or was narrower after catalytic treatment.  
24 Tessarolo *et al.*<sup>22</sup> used <sup>1</sup>H NMR, GCxGC-TOFMS, and (-) ESI FT-ICR MS to characterize  
25 sugarcane bagasse and pinewood pyrolysis bio-oils before and after catalytic treatment on  
26 zeolite. Deoxygenation efficiency of the catalytic process was assessed by an increase of the  
27 relative abundance of less oxygenated compounds. However, the limitation of using only the  
28 negative ESI mode to the description of the catalytic treatment of the bio-oil was highlighted  
29 in previous works.<sup>23,24</sup> We have combined (-) ESI and LDI FT-ICR MS to analyze the heavy  
30 species present in lignin pyrolysis bio-oils as a function of catalytic treatments. Considering  
31 the results obtained by the petroleomic approach, we have evidenced the importance of the  
32 ionization source on the description of the bio-oil composition to understand the HDO  
33 treatment effect. Therefore, LDI was a suitable ionization source to assess the species from  
34 upgraded bio-oils as they are expected to be less polar and less saturated than those of the  
35 raw bio-oil. Moreover, we have recently demonstrated that the combination of the ESI, APPI,  
36  
37  
38  
39  
40  
41  
42  
43  
44  
45  
46  
47  
48  
49  
50  
51  
52  
53  
54  
55  
56  
57  
58  
59  
60

1  
2  
3 and LDI with FT-ICR MS analyses for the characterization of a lignocellulosic pyrolysis bio-oil  
4 increased the coverage of the sample description.<sup>25</sup>  
5  
6  
7

8 By means of this new analytical method, we propose to assess the selectivity of two  
9 different zeolites toward the heavy compounds produced by the CFP of oak. The first  
10 catalyst is a conventional HZSM-5 zeolite, and the second one is a hierarchical zeolite  
11 produced by desilication with NaOH solution of the first one.  
12  
13  
14

## 15 16 **MATERIALS AND METHODS**

### 17 **BIO-OILS PRODUCTION**

#### 18 **Biomass sample**

19  
20  
21 In this study, the bio-oils were obtained by pyrolysis of cylinder particles of oak. Oak  
22 was harvested in the Haut-Beaujolais area (South-East France). All cylinder particles (o.d. 6  
23 mm × 20 mm) were milled from the same piece of oak, in the heartwood zone, on the same  
24 radius and with their length in the direction of the fibers. The mass of the cylinder was 0.65 g  
25 (+/- 0.2 g). The moisture content of the injected wood cylinders was 7wt % The mass of one  
26 cylinder on anhydrous basis was 0.60 g (+/- 0.2 g). More details about the sampling  
27 procedure and the composition of this biomass are available elsewhere.<sup>26–28</sup>  
28  
29  
30  
31  
32  
33  
34

#### 35 **Fast pyrolysis experiments**

36  
37  
38 The pyrolysis experiments were performed at CNRS Nancy, in a microfluidized bed  
39 reactor set at 500 °C. More information about the design and operation of the reactor are  
40 reported in different studies.<sup>26,28,29</sup> Oak cylinders were injected in stepwise mode and the  
41 vapors were condensed in three cold traps (with methanol). The effect of particle size on the  
42 pyrolysis regime has been studied in our previous work.<sup>30</sup> Our particle size (6/4=1.5mm  
43 characteristic length) is relevant for studying biomass fast pyrolysis in fluidized bed  
44 reactors.<sup>31,32</sup>  
45  
46  
47  
48  
49  
50

51  
52 The injection of one cylinder represents a biomass-to-catalyst ratio of around 0.12 (0.6/5 g).  
53 Therefore, this size of particle presents a good trade-off between a relevant pyrolysis regime  
54 and mass of samples (bio-oil, coke, etc.) for further analyses.  
55  
56  
57  
58  
59  
60



1  
2  
3 Upgraded bio-oils were produced with parent (A) or hierarchical (B) HZSM-5 zeolites.  
4 The latter was produced in Poitiers following a previously published procedure.<sup>29,33</sup> First, 5 g  
5 of zeolite were introduced in the fluidized bed and were pre-treated under nitrogen. Then,  
6 14 oak cylinders were injected, which corresponds to a biomass-to-catalyst ratio of 1.7. The  
7 liquid bio-oil obtained from the pyrolysis of the first seven cylinder was collected  
8 (corresponding to a biomass-to-catalyst ratio of 0.85) and diluted in ~100 mL of methanol  
9 (“bio-oil solution”). Then, the 8 to 14 cylinders were stepwise injected and a second bio-oil  
10 solution was obtained.  
11 Finally, five different samples were obtained in respect with the experimental conditions:  
12 the raw bio-oil (obtained with silica sand as a bed material) and upgraded A 1-7, A 8-14, B 1-  
13 7, and B 8-14 bio-oils.  
14  
15  
16  
17  
18  
19  
20  
21

### 22 **SAMPLE PREPARATION**

23  
24 The used solvents and chemicals, methanol (VWR–Prolabo), water (Fisher Chemical), and  
25 sodium acetate (Fisher Scientific) were LC MS grade and used as supplied. For (-) ESI and (+)  
26 APPI analyses, the different bio-oil solutions were diluted up to 50 and 25 times,  
27 respectively, in methanol without addition of dopant. For the analyses in (+) ESI, the bio-oil  
28 solutions were 100 times diluted in methanol containing sodium acetate (0.1 mg.mL<sup>-1</sup>) to  
29 improve cationization processes as previously shown in our previous work.<sup>25,34</sup> For LDI  
30 measurements, 1 µL of bio-oil-was deposited on a stainless steel target and dried at room  
31 temperature.  
32  
33  
34  
35  
36  
37  
38  
39  
40

### 41 **FOURIER TRANSFORM ION CYCLOTRON RESONANCE MASS SPECTROMETER**

42  
43 The measurements were performed on a 12 T SolariX FT-ICR equipped with ESI and APPI  
44 sources (Bruker Daltonics). The software FTMSControl V2.1.0, build 98 (Bruker Daltonics)  
45 was used to optimize the different ionization methods and operating parameters. For LDI  
46 analyses, a 9.4 T FT-ICR mass spectrometer (IonSpec/Varian) fitted with a specific LDI card  
47 was used.  
48  
49  
50  
51

### 52 **ESI FT-ICR MS**

53  
54 The analyses were carried out in both positive and negative ion modes. The voltages of  
55 the end plate and the capillary were set at – 500 and ± 4000 V, respectively. The source gas  
56  
57  
58  
59  
60

1  
2  
3 was heated at 180 °C and tuned with nebulizer gas (1.8 - 2 bar) and dry gas (4 – 6 L.min<sup>-1</sup>).  
4 The infusion flow rate of the sample was 200 μL.h<sup>-1</sup> into the ion source. The ions were  
5 accumulated for 0.3 s per scan and 200 scans were summed to achieve the final mass  
6 spectrum that was ranging from *m/z* 129 to 600. The length of the transient was 3 s and the  
7 mass resolution was ~ 680 000 at *m/z* 400.  
8  
9  
10

### 11 **APPI FT-ICR MS**

12  
13  
14 The APPI source used for the analyses is equipped with a Krypton lamp which emits 10.6  
15 eV energy photons. The capillary voltage was set at - 987 V and the end plate at – 500 V. The  
16 source gas was tuned with nebulizer gas (1.8 bar) and dry gas (6 L.min<sup>-1</sup>) and heated at 180  
17 °C. The samples were infused at a flow rate of 1 mL.h<sup>-1</sup> and the ions accumulated for 0.05 s.  
18 The sum of 100 scans was done to obtain the final mass spectrum in the *m/z* 129 to 1000  
19 range. The transient length was 1.5 s and the mass resolution was ~ 340 000 at *m/z* 400.  
20  
21  
22  
23

### 24 **LDI FT-ICR MS**

25  
26  
27 The LDI measurements were achieved in negative ion mode by using a laser desorption  
28 ionization LDI FT-ICR mass spectrometer (IonSpec, Lake Forest, CA) equipped with an actively  
29 shielded 9.4 Tesla superconducting magnet (Cryomagnetics, Oak Ridge, TN). Laser  
30 desorption ionization is performed by a Nd:YAG ORION air-cooled laser system (New Wave  
31 Research Inc, Fremont, CA) working at the 355 nm wavelength (laser pulse duration 5 ns,  
32 output energy 4 mJ) in an external ion source before transfer by an ion guide to the ICR cell  
33 where they are analyzed. Height laser shots were accumulated per scan. Forty five scans  
34 were summed to obtain the final mass spectrum that ranges from *m/z* 150 to 800. The  
35 transient length is 1.05 s and the resolving power ~ 150 000 at *m/z* 400. The power of the  
36 laser was optimized to avoid fragmentation and recombination phenomenon.  
37  
38  
39  
40  
41  
42  
43  
44  
45

### 46 **DATA POST-ACQUISITION TREATMENT**

47  
48 The mass spectra obtained in ESI and APPI FT-ICR MS were analyzed with Data Analysis  
49 V4.4, build 102.47.2299 (Bruker Daltonics) and calibrated with a peak list, generated for each  
50 analytical condition, of well-known oxygenated compounds whose S/N ratio was greater  
51 than 4. To assign a molecular formula to each signal, PetroOrg software (Florida State  
52 University) was used with the following attribution parameters C<sub>1-100</sub>H<sub>2-200</sub>O<sub>1-20</sub>N<sub>0-20</sub>S<sub>0-1</sub> (for  
53  
54  
55  
56  
57  
58  
59  
60

negative ion mode) and  $C_{1-100}H_{2-200}O_{1-20}N_{0-20}S_{0-1}Na_{0-1}$  (for adducts in positive ion mode). The tolerated mass error was  $\pm 1$  ppm.

For 9.4 T LDI FT-ICR MS measurements prior to acquisition, the mass spectrometer was externally calibrated by considering well-known ions such as hydride gold cluster ions. Following acquisition, internal calibration was performed with specific and well characterized  $C_xH_yO_{3,4,5}^{+/-}$  ion series. A peak list of signals with a S/N > 4.5 was generated and the Composer software (Sierra Analytics, Modesto, CA) was used for ion assignment with the following search criteria:  $C_{1-100}H_{1-100}N_{0-2}O_{1-30}S_{0-1}$  general formula, 3 ppm tolerance error, and a double bound equivalent (DBE) ranging from 0 to 40. The recalibration of the mass spectrum was then conducted with signals assigned with an error lower than 1 ppm by considering the **Equation (1)**.

$$\frac{m}{z} = \frac{A}{f} + \frac{B}{f^2} \quad (1)$$

Whatever the analytical conditions, the graphical representation of the mass error against  $m/z$  and the value of the RMS of the mass error ensure to check the right assignation of the different signals and the good calibration of the mass spectrum. They are available in the **Table S1** and **Figure S1** (*Supporting information*). Due to the significant number of peaks composing the mass spectrum, graphical representations were used to compare the results achieved whereby the sample and the analytical conditions. Among them, van Krevelen diagram represents each molecular formula  $C_xH_yN_nS_sO_z$  in the form of dot whose x and y coordinates represent O/C and H/C ratios, respectively. From this graph, biomass component derivatives can be highlighted. Hence, lipids (low O/C and H/C  $\sim 2$ ), sugarc derivatives (high O/C and H/C ratios) and products from lignin pyrolysis (H/C  $\sim 1$  and O/C between 0.2 and 0.6) can be distinguished (**Figure S2**).

## RESULTS AND DISCUSSION

First of all, whatever the analyzed bio-oil sample, the compounds detected by ESI are sodium adducts  $[M+Na]^+$ , in positive ion mode, and deprotonated ions  $[M-H]^-$ , in negative ion mode. By (+) APPI, both radical and protonated ions are detected, and by (-) LDI, deprotonated ions and, to a lesser extent, radical ions are detected. Using different ionization conditions for the analysis of bio-oils ensures to take advantage of the

1  
2  
3 petroleomic approach.<sup>25,35,36</sup> The formula of each detected ion is considered for the  
4 comparison of chemical composition of raw and upgraded bio-oils.  
5

6 In a first part, the effect of the nature of the catalyst on the heavy bio-oil fraction from  
7 CFP of oak is achieved by comparing the results obtained with the catalysts noted A (parent  
8 zeolite) and B (hierarchical zeolite), and with silica sand (noted "Raw BO"). Thus, the  
9 comparison was conducted with the upgraded bio-oils from the fast-pyrolysis of the first  
10 seven oak cylinders as representative of the catalyst effect (samples A 1-7 and B 1-7).  
11  
12  
13

14 In a second part, the upgraded bio-oils, from the last 7 injections (8-14) of oak cylinders,  
15 were considered to investigate the catalyst lifetime on the composition of the generated  
16 bio-oils (samples A 8-14 and B 8-14).  
17  
18  
19  
20  
21  
22

## 23 **EFFECT OF THE TYPE OF CATALYST ON THE HEAVY SPECIES COMPOSITION OF THE BIO- 24 OIL**

### 25 **Composition of the raw bio-oil**

26  
27 As we demonstrated before<sup>25</sup>, a raw bio-oil (without catalyst), from pyrolysis of  
28 lignocellulosic material, may be extensively described by using compositional data obtained  
29 by (+/-) ESI, (+) APPI, and (-) LDI FT-ICR MS. This combining approach applied to this raw bio-  
30 oil from oak pyrolysis, gives the same description. The achieved bio-oil composition gives  
31 close to 90 % of the total ion current (TIC) attributed to  $C_xH_yO_z$  compounds (**Table 1**) and the  
32 remaining part of the signal is attributed to  $C_xH_yNO_z$  and  $C_xH_ySO_z$  species. Sulphur containing  
33 species are only observed in negative ion mode analyses (8 % of the TIC by ESI and 9 % by  
34 LDI) whereas nitrogen compounds are observed in ESI (8 %) and APPI (1 %), in positive ion  
35 mode. The distributions of the  $C_xH_yO_z$  compounds in respect with their oxygen atom count  
36 are ranging from 0 to 13 with maximum for  $O_4$  to  $O_6$  species (**Figure 1**). In (+) ESI, a bimodal  
37 distribution is obtained with the first massif centered on  $O_5$  and the second one, on  $O_{10}$ . This  
38 shape was described in a previous work.<sup>34</sup> The first massif, which corresponds to lignin  
39 derivatives as well as lipids, is also described by (-) ESI, (+) APPI, and (-) LDI analyses. The  
40 second one is less intense, more specifically detected by (+) ESI, and is attributed to pyrolytic  
41 sugarc derivatives. The representations of the  $C_xH_yO_z$  formulae on van Krevelen diagrams  
42 enable to highlight these different biomass derivatives (**Figure 2**).  
43  
44  
45  
46  
47  
48  
49  
50  
51  
52  
53  
54  
55  
56  
57  
58  
59  
60

1  
2  
3 Finally, as expected, a large panel of components of the raw bio-oil heavy fraction are  
4 extensively described by this analytical method. This is a prerequisite to investigate the  
5 selectivity of the catalysts used for CFP of oak.  
6  
7

### 8 **Effect of the zeolites on the bio-oil composition**

9

10  
11 In addition to raw bio-oil data, the **Table 1** displays the relative abundance of the  $C_xH_y$ ,  
12  $C_xH_yO_z$ ,  $C_xH_yNO_z$ , and  $C_xH_ySO_z$  compound families identified in (+/-) ESI, (-) LDI, and (+) APPI  
13 FT-ICR MS for upgraded bio-oils. Overall, close to 90 % of the TIC is due to  $C_xH_yO_z$   
14 compounds. The other contributions are nitrogen and sulphur species which are mainly  
15 observed in positive and negative ion modes, respectively. However, some different trends,  
16 depending on the analytical conditions, can be shown. In addition to  $C_xH_yO_z$  compounds,  
17 pure hydrocarbons,  $C_xH_y$ , are specifically detected by (-) LDI and (+) APPI. Moreover, the  
18 number of identified formulae in bio-oils can be similar or higher than in the raw bio-oil, this  
19 is the case for (-) ESI, (-) LDI, and (+) APPI analyses whereas in (+) ESI, they are three times  
20 less numerous.  
21  
22

23  
24 The distribution of the  $C_xH_yO_z$  and  $C_xH_y$  compounds in respect with the oxygen atom  
25 content is displayed in the **Figure 1**. The ranges obtained for the upgraded bio-oils are  
26 slightly narrower and shifted to lower values of oxygen atoms. **Figure 1** also indicates that  
27 the distribution of the chemical families is greatly dependent on the used ionization  
28 condition. APPI and LDI seem to show similar trends in regard to the detected chemical  
29 families of upgraded bio-oils whereas (+) and (-) ESI reveal different features.  
30  
31

32  
33 Therefore, for all these reasons, it is necessary to have a deeper insight into the  
34 differences observed between the raw and the upgrading bio-oil compositions for each  
35 analytical condition before giving a real view of the selectivity of the catalysts.  
36  
37

38  
39 In (+) ESI, the abundances of the oxygen-poor compounds ( $O_1$ ,  $O_2$ , and  $O_3$ ) are greater in  
40 the upgraded bio-oils, more especially in the B one, than in the raw bio-oil. The upgraded  
41 bio-oils contain species with up to 10 oxygen atoms and the second massif previously  
42 observed in the raw bio-oil distribution is no longer present in the upgraded bio-oil samples.  
43 This change relative to the catalytic treatment is attested on the van Krevelen diagrams.  
44 Indeed, the area corresponding to the sugarc derivatives species is almost empty for the  
45 bio-oils A 1-7 and B 1-7 (**Figure 2**). It means that these compounds are well converted by the  
46 two catalysts. Concerning the pyrolytic lignin derivatives, they are detected in the 3 samples  
47 but their O/C and H/C ratios are shifted to lower values when a catalyst was used, especially  
48  
49  
50  
51  
52  
53  
54  
55  
56  
57  
58  
59  
60

1  
2  
3 in the sample B 1-7. In the **Figure 1**, the relative abundances of the O<sub>6</sub> species are still  
4 significant, even in the catalytic bio-oils. Nevertheless, their distribution regarding the DBE  
5 value are quite different depending on the sample (**Figure S3**). Low unsaturated compounds  
6 (with DBE=2 prominent) are specifically detected in the raw bio-oil whereas more  
7 unsaturated ones are detected in upgraded samples. This difference is even pronounced  
8 when the number of oxygen atom per molecules increases until O<sub>11</sub>-O<sub>12</sub>, which are only  
9 detected in the raw bio-oil. Looking at the DBE distribution of the low oxygenated  
10 compounds, (O<sub>1</sub>, O<sub>2</sub>, and O<sub>3</sub>, **Figure S3**) new aromatic compounds are formed due to  
11 catalytic treatment, especially with the catalyst B, and are characterized by #C 10 - 22.

12  
13  
14  
15  
16  
17  
18 The results achieved in (-) ESI show, for the C<sub>x</sub>H<sub>y</sub>O<sub>z</sub> and C<sub>x</sub>H<sub>y</sub> compounds classes, a nearly  
19 similar range of the oxygen atom count between the bio-oil samples (**Figure 1**) even if the  
20 number of assignments is half more important in upgraded bio-oils (**Table 1**). However, if the  
21 O<sub>4</sub> compounds are prominent in the 3 samples, the species having 2 to 5 oxygen atoms are  
22 more abundant in the bio-oil A 1-7 and, to a lesser extent in the B 1-7, than in the raw bio-  
23 oil. Inversely, the O<sub>6</sub> to O<sub>13</sub> compounds are more abundant in the raw sample. A unique  
24 behavior is observed for the upgraded bio-oil B 1-7 for which the O<sub>2</sub> species are dramatically  
25 detected. A deep insight into this compound family demonstrates that they correspond to  
26 pyrolytic lignin derivatives. Among them, the most abundant species have DBE=6 and  
27 contain between 10 and 15 carbon atoms. These features are close to those of phenolic  
28 species. Nevertheless, whatever the used catalyst, these compounds are the main peaks  
29 detected in negative ion mode by ESI and will be discussed later. The van Krevelen diagrams  
30 obtained for the upgraded bio-oils look similar to the raw one (**Figure 2**). However, new  
31 compounds at very low O/C values appear, which indicates a partial deoxygenated effect of  
32 both catalysts. Splitting these data and looking at the DBE distribution according to the  
33 number of carbon atoms for each O<sub>z</sub> family allows to confirm this trend (**Figure S4**). Both  
34 catalysts show the same effect on bio-oil. Apart from the most oxygenated species which are  
35 only detected in the raw bio-oil (O<sub>11</sub> - O<sub>12</sub>), the compounds identified in the raw bio-oil are  
36 also detected when a catalyst was used during pyrolysis. Nonetheless, for catalytic bio-oils,  
37 their distribution is extended to higher unsaturation range and higher number of carbon  
38 atoms. This is specifically the case for O<sub>2</sub>-O<sub>5</sub> classes. This demonstrates the appearance of  
39 new heavy oligomeric compounds which are aromatic and less oxygenated. Furthermore,  
40 increasing aromaticity of acidic compounds may drastically increase their ability to be  
41  
42  
43  
44  
45  
46  
47  
48  
49  
50  
51  
52  
53  
54  
55  
56  
57  
58  
59  
60

deprotonated and detected in negative ESI.<sup>37</sup> New light  $O_1$  compounds are also specifically detected in the CFP bio-oils.

In APPI (+), the number of detected mass peaks is higher for A 1-7 sample than for the raw one and the B 1-7 sample (Table 1). The range of the distribution of the  $C_xH_yO_z$  compounds, in respect with the oxygen atom number, is clearly shifted to lower values when a catalyst was used, especially with the hierarchical zeolite (catalyst B, see Figure 1). Thus, while the contribution of the most oxygenated compounds dropped in the catalytic bio-oils, the  $C_xH_y$  and  $O_1$ - $O_4$  components are prominent in the sample B 1-7, and, to a lesser extent, in the bio-oil A 1-7. This trend is also observable in the Figure 2 where only pyrolytic lignin and lipids are detected. Regarding the point cloud of the lignin derivatives, it is more intense in the lower  $O/C$  values when a catalyst is used, more especially with the hierarchical one. Moreover, this effect is balanced by the emergence of some new  $C_xH_y$  compounds. These compounds have a DBE ranging from 6 to 21 and a #C from 11 to 29 which indicates their aromatic feature (Figure 3). A similar distribution of  $O_1$  compounds are also specifically detected on upgraded bio-oils (Figure 4). Saturated or poor unsaturated lipids ( $O_1$ - $O_4$  and DBE = 0-5) are also detected and seem to be not impacted by the catalytic treatment. The Figure 4 shows that raw bio-oil and bio-oil A 1-7 are quite similar in terms of number of carbon atoms and DBE range for  $O_4$  -  $O_{10}$  species. For each #C, additional compounds of the sample A 1-7 are detected at a DBE+1 value at the top of the distribution of the raw bio-oil compounds. In the sample B 1-7, the high mass and high unsaturated compounds have been removed from  $O_7$  to  $O_{11}$  families. Thus, these specific compounds are clearly more reactive towards the hierarchical zeolite than to the parent one.

The differences between raw and upgraded bio-oil compositions observed in (-) LDI FT-ICR MS are comparable to those achieved in (+) APPI but at higher and complementary DBE values. The  $C_xH_yO_z$  compounds contained less oxygen atoms in the upgraded bio-oils than in the raw one (Figure 1). The detected species of the three bio-oil samples have from 0 to 8 oxygen atoms. However, the relative abundances attributed to  $C_xH_y$  and  $C_xH_yO_z$  ( $z=1-3$ ) compounds are higher in the catalyzed samples than in the raw one, especially for  $O_1$ ,  $O_2$ , and  $O_3$  in the sample B 1-7. The most oxygenated species (with  $z > 5$ ) are more intensely detected in the raw bio-oil. These results are coherent with the van Krevelen diagrams of these compound families (Figure 2). Pyrolytic lignin is commonly identified in all experiments. Nevertheless, some changes can be highlighted. In fact, after catalytic

1  
2  
3 treatment, these components are less oxygenated, which is illustrated by a shift of the point  
4 cloud to lower O/C ratio values. This observation is slightly more pronounced for the bio-oil  
5 B 1-7. By displaying the DBE values of detected compounds according to the number of  
6 carbon atoms, the (-) LDI analyses give details on the aromatic range of hydrocarbons (**Figure**  
7 **3**). Specifically in the sample B 1-7, a significant distribution is highlighted which is extended  
8 to high value of DBE and high number of carbon atoms (high masses). This suggests a specific  
9 capacity of the B catalyst to produce and release such heavy polycyclic aromatic  
10 hydrocarbons (PAH) in the gas phase. For all the O-classes, catalyst B generates more  
11 unsaturated species than the raw and the A 1-7 bio-oils (**Figure S5**).  
12  
13  
14  
15  
16  
17  
18  
19

20 Finally, integrating the results obtained by petroleomic approach using different ion  
21 sources leads to reveal several effects of the zeolite catalysts on the heavy fraction of the  
22 bio-oil. A high deoxygenation effect is firstly marked by the removal of the sugarc species  
23 derived from cellulose and hemicellulose which are no more detected (notably by (+) ESI).  
24 This effect, observed for parent and hierarchical HZSM-5, is balanced by an increase of the  
25 number of compounds relative to lignin derivatives (**Figure 2**). For these latter bio-oil  
26 components, their oxygen proportion (O/C) drops and O<sub>1</sub>-O<sub>5</sub> compounds arise, as it is  
27 particularly highlighted by (+) APPI, (-) ESI, and (-) LDI. This demonstrates that these bio-oil  
28 components are from lignin oligomers.  
29  
30  
31  
32  
33  
34

35 The most oxygenated species (O<sub>10</sub> to O<sub>13</sub>) which are in the highest mass range of the  
36 lignin derivatives disappear when a catalyst is used. Nevertheless, some of them, at high DBE  
37 value (DBE=10-25) and with a high carbon atom count (#C > 15), are still detected when  
38 parent zeolite is used but are no longer detected in the bio-oil upgraded with the  
39 hierarchical zeolite (**Figure 4**).  
40  
41  
42  
43

44 Concerning the moderate oxygenated compounds of the lignin derivatives (O<sub>6</sub> to O<sub>9</sub>),  
45 their distribution in mass and DBE are very close to those detected in the non-catalyzed  
46 pyrolysis bio-oil and differ mainly by their abundances. It has to be noted that with the  
47 hierarchical zeolite, the most unsaturated oxygen-containing compounds are less detected  
48 than with the parent zeolite (by (+) APPI). A specific behavior of the parent zeolite, and to a  
49 lesser extent of the hierarchical one, is observed for these compounds. Systematically, for a  
50 same O-class and a given #C series, the detected compounds have higher DBE values, at  
51  
52  
53  
54  
55  
56  
57  
58  
59  
60



1  
2  
3 least, by 1 unit compared to raw bio-oil. Cyclization reaction is therefore suspected to induce  
4 this additional unsaturation.  
5

6 For O<sub>2</sub> to O<sub>5</sub> compounds, apart from the most saturated compounds which are still  
7 detected (associated to “lipids”), the CFP bio-oils contain not only the same compounds than  
8 in the raw bio-oil but also new compounds at higher number of carbon atoms and DBE  
9 values. This is more pronounced with the hierarchical zeolite. These polyaromatic  
10 compounds containing 2, 3, 4, and 5 oxygen atoms appear to be correlated with the loss of  
11 higher mass compounds which contain more oxygen and carbon atoms and have similar or  
12 lower DBE value. It suggests that the decomposition of lignin products is promoted by the  
13 catalyst by a concomitant removing of oxygen groups and an increase of aromaticity. This  
14 effect is more noticeable when the catalyst contains mesopores. Aromatization on  
15 hierarchical zeolites is suggested to be the main deoxygenation mechanism of bio-oils.  
16 Interesting behavior is observed for C<sub>x</sub>H<sub>y</sub>O<sub>2</sub> compounds with DBE=6. These C<sub>10</sub>-C<sub>16</sub> molecules  
17 are more intensely detected by (-) ESI whatever the used catalyst (Figure S6). Even if their  
18 signals in (+) APPI is less significant than in (-) ESI (on the basis that they correspond to the  
19 same compounds), they remain predominant with the catalyst B. In (+) ESI, these  
20 compounds are the most strongly detected in the bio-oil B 1-7 as [M+Na]<sup>+</sup> ions. This suggests  
21 that these species contain either carboxylic group or two vicinal oxygen group, such as an  
22 aldol, able to interact with a sodium ion. The C<sub>10</sub> ions have been also intensely detected in  
23 bio-oils by Bi *et al.*<sup>38</sup> and Tessarolo *et al.*<sup>22</sup> They were attributed to a phenol fused with a  
24 cyclohexanone. This is in accordance with its ability to be ionized by sodium adduct. This  
25 group of O<sub>2</sub> compounds may then correspond to intermediate catalytic products involving a  
26 phenolic group and a cyclohexanone-type moiety. Nevertheless, even if the zeolite is known  
27 to promote decarboxylation, we cannot neglect the contribution of an aromatic carboxylic  
28 acid. Indeed, a very interesting study intended to rationalize the ionization efficiency of  
29 some model polar compounds with different ion sources.<sup>37</sup> They demonstrated that isomeric  
30 carboxylic acids with DBE=6 have a dramatic different ionization efficiency in negative ESI  
31 depending on the isomer structure.  
32  
33  
34  
35  
36  
37  
38  
39  
40  
41  
42  
43  
44  
45  
46  
47  
48  
49  
50

51 Except a group of compounds those formulae may be linked to triterpenols or  
52 triterpenoids (area at #C from 27 to 30 and DBE=6-11), O<sub>1</sub> compounds are aromatics and  
53 polyaromatics. They are exclusively formed during catalytic pyrolysis and are systematically  
54 the lower mass compounds of the total distribution (O<sub>1</sub> by (+) APPI, (+/-) ESI, and (-) LDI in  
55  
56  
57  
58  
59  
60

1  
2  
3 **Figures 4, S3, S4, and S5**, respectively). This result observed for the poor oxygenated  
4 catalytic products is also extended to the pure hydrocarbons. Apart from compounds  
5 associated to triterpene-like hydrocarbons (with one or more unsaturation, area at #C from  
6 27 to 31 and DBE=6-13), new pure hydrocarbon products appear specifically in the  
7 composition of these catalyst bio-oils ( $C_xH_y$  with #C from 10 to 40 with DBE=6-34) (**Figure 3**).  
8 They correspond to aromatic and polyaromatic hydrocarbon compounds (PAH and alkyl-  
9 PAH) whose range of degrees of aromaticity depends on the nature of catalyst. The ability of  
10 HZSM-5 catalyst to produce heavy aromatics is evidenced. The reaction network leading to  
11 their generation involves numerous routes depending on the bio-oil component.<sup>15</sup> Diels  
12 Alder reaction between light compounds, such as furans and olefins<sup>39</sup>, may conduct to large  
13 aromatics. This is what it is observed, in particularly, with the hierarchical catalyst which  
14 leads to compounds with a broader range of aromaticity (DBE value can be as high as 34).  
15 This is one of the major differences between the parent and the hierarchical zeolite. This  
16 finding reveals that the mesopores formed by desilication can promote the formation of  
17 heavy pure hydrocarbons. The pore network in the hierarchical zeolite may enhance the  
18 transport and the release of a broader range of compounds from the zeolite crystallites.  
19 These heavy hydrocarbons could be important precursors of coke in zeolite, which is  
20 currently a problem in CFP. Indeed, it limits the activity of the catalyst by blocking the  
21 accessibility of the active acidic sites. Nevertheless, the presence of mesoporous structures  
22 in the hierarchical zeolite may reduce the formation of toxic coke<sup>29,40</sup> by promoting the  
23 transport of heavy hydrocarbons to the external surface of zeolite particles. The stability of  
24 both zeolites in regards to coke deposit is the purpose of the next section.

## 42 **MONITORING OF THE CATALYST LIFETIME**

43  
44  
45 The evolution of the composition of the bio-oils obtained by the pyrolysis of the 8 to 14  
46 oak cylinders gives insights on the stability of both catalysts.

47  
48  
49 The bio-oils A 8-14 and B 8-14 were analyzed by applying the same methodology used for  
50 the characterization of the raw, A 1-7, and B 1-7 bio-oils. As previously observed for the A 1-  
51 7 and B 1-7, the signal is mainly assigned to  $C_xH_yO_z$  ( $z=1-12$ ) compound class with relative  
52 abundance close to 90 % (**Table 1**). Minor compounds corresponding to  $C_xH_yNO_z$  and  $C_xH_ySO_z$   
53 families (from 0 to 10 % and from 1 to 9 % of the TIC, respectively) are also assigned.  
54  
55  
56  
57  
58  
59  
60

1  
2  
3 However the signal abundance of the  $C_xH_y$  falls to maximum 3 % (by (+) APPI). The number of  
4 signals in B-catalyzed bio-oil are nearly the same from 1-7 to 7-14 samples, an increase is  
5 observed in the bio-oil A (see by (+) ESI and (-) LDI).  
6  
7

8 The  $C_xH_yO_z$  compounds from the bio-oil A 8-14 contain up to 12 oxygen atoms against 11  
9 for the bio-oil A 1-7 (Figure 1). Overall, the intensities of the most oxygenated compounds  
10 are more significant in the sample A 8-14 whereas the less oxygenated ones are more  
11 abundant in the sample A 1-7. Furthermore, the bimodal distribution is obtained in (+) ESI  
12 with the upgraded bio-oil A 8-14 as with the raw bio-oil. This second massif is attributed to  
13 sugarc derivatives whose presence is confirmed by the (+) ESI van Krevelen diagram (Figure  
14 5). These biomass components are significantly more represented in this sample than in the  
15 A 1-7 one. Lipids are evidenced on the van Krevelen diagrams obtained by (-) ESI and (+) APPI  
16 analyses. Lignin derivatives are highlighted on all diagrams. Nevertheless, in (+) APPI and (-)  
17 LDI, some  $C_xH_yO_z$  formulae are plotted with a higher O/C ratio than in the bio-oil A 1-7.  
18  
19  
20  
21  
22  
23  
24  
25

26 For the sample B 8-14, similar observations can be done. The oxygen-poor species are  
27 more abundant in the bio-oil B 1-7 whereas in the bio-oil B 8-14, the relative abundances of  
28 the most oxygenated species are higher (Figure 1). However, the range is not different  
29 between the two samples, which is attested by the van Krevelen diagrams (Figure 5). Indeed,  
30 the plotted  $C_xH_yO_z$  compounds do not present a higher O/C ratio. These diagrams are very  
31 close to those obtained with the bio-oil B 1-7. Thus, lipids are highlighted in (-) ESI and (+)  
32 APPI and lignin derivatives, in all measurements. Sugarc components are still not detected in  
33 this sample, which demonstrates that the mesoporous zeolite is still active for sugarc  
34 compounds conversion even at the high biomass-to-catalyst ratios.  
35  
36  
37  
38  
39  
40

41 Thorough comparison of the catalytic response, displaying the DBE vs. the number of  
42 carbon atoms, clearly evidences the deactivation of parent HZSM-5 and the sustainable  
43 efficiency of the hierarchical one (Figures S7, S8, S9, and S10). Bio-oil produced by CFP with  
44 HZSM-5 catalyst highlights nearly the same compounds as those observed in the raw bio-oil  
45 whatever the ionization and detection mode. Inversely, CFP with hierarchical catalyst still  
46 evidences a loss of numerous highly oxygenated compounds as it was observed for the first  
47 1 to 7 wood injections. Nevertheless, pure hydrocarbons are less abundant and their  
48 unsaturation degree is less extended ( $DBE_{max} = 18$ , Figure 3).  
49  
50  
51  
52  
53  
54

55 The diminution of the effectiveness after several pyrolysis runs also illustrates the  
56 deactivation of the parent zeolite due to coke deposit. The carbon deposition occurring in  
57  
58  
59  
60

1  
2  
3 the micropores may block the access of the bio-oil compounds to acidic sites for  
4 deoxygenation reactions.<sup>29,41</sup> Nevertheless, some active sites are still accessible even after  
5 coking for hierarchical zeolite whose mesoporous structure balances the limitation of the  
6 microporous diffusion.<sup>42</sup> The consequence is a more stable activity of hierarchical catalyst to  
7 produce compounds with higher aromaticity even at high biomass-to-catalyst ratio.  
8  
9  
10

11  
12  
13 Finally, all these results give some insights into the zeolite effect on the pyrolysis of  
14 lignocellulosic biomass. During biomass pyrolysis, the oxygenated volatiles interact with  
15 zeolites to form light species which could form aromatics over Brønsted active sites located  
16 in micropores and coke precursors located within the pores in crystals.<sup>29</sup> Depending on the  
17 porous structure of crystals, these precursors could migrate up to the external surface of  
18 crystal or be entrapped within the crystals. In hierarchical zeolite, the migration of these  
19 coke precursors to the external surface may be promoted thanks to the mesopores  
20 produced after desilication and to a higher external surface.<sup>29,43,44</sup> The promotion of the  
21 migration of coke precursors for the hierarchical zeolite may explain the highest yield in  
22 heavy hydrocarbons released (up to 40 carbons) and detected in bio-oils by our high  
23 resolution MS method. The mechanisms of mass transfers within hierarchical zeolite under  
24 significant conditions of biomass fast pyrolysis in a fluidized bed needs to be further  
25 investigated to confirm this hypothesis.  
26  
27  
28  
29  
30  
31  
32  
33  
34  
35  
36

## 37 CONCLUSION

38  
39 Petroleomic approach on heavy bio-oil compounds allows to assess the selectivity of  
40 catalysts used during CFP of biomass. An efficient deoxygenation process is particularly  
41 evident for sugarc compounds and some oxygen-rich lignin derivatives. Nevertheless, a  
42 major part of the lignin pyrolysis products is refractory to deoxygenation. Pure heavy  
43 hydrocarbons are generated especially by the hierarchical zeolite (even with biomass-to-  
44 catalyst ratio up to 0.85). It is clearly demonstrated that the parent zeolite has few effects on  
45 the heavy products compared to the hierarchical one. These products exhibit a poor  
46 interaction with the parent zeolite because they cannot access to its micropores.  
47 Furthermore, the parent catalyst is more quickly deactivated than the hierarchical one,  
48 which demonstrates deoxygenation efficiency even at high biomass-to-catalyst ratio. These  
49 findings reveal that additional mesopores on microporous HZSM-5 improves the biomass  
50  
51  
52  
53  
54  
55  
56  
57  
58  
59  
60

1  
2  
3 catalytic pyrolysis to produce heavy compounds with higher aromaticity and lesser oxygen-  
4 containing.  
5  
6  
7

## 8 **ACKNOWLEDGEMENT**

9  
10 The authors, more especially Jasmine Hertzog, would like to thank the European COST Action  
11 1306 “Lignoal” for its financial support. It enabled a new collaboration between the LCP-  
12 A2MC and the LRGP, University of Lorraine, and the UK Biochar Research Center, University  
13 of Edinburgh. The measurements carried out with the 12 T FT-ICR MS were done at the  
14 Scottish Instrumentation and Resource Centre for Advanced Mass Spectrometry (SIRCAMS)  
15 at the University of Edinburgh. The TGIR program FR 3624, infrastructure program of CNRS,  
16 is acknowledged for further financial support.  
17  
18  
19  
20  
21  
22

## 23 **SUPPORTING INFORMATION**

24  
25 General information on mass peak assignment, graphical representations of compounds  
26 detected in the different experimental conditions (catalyst, ion source)  
27  
28  
29  
30  
31  
32  
33

## 34 **REFERENCES**

- 35  
36 (1) Moss, R. H.; Edmonds, J. A.; Hibbard, K. A.; Manning, M. R.; Rose, S. K.; van Vuuren, D. P.;  
37 Carter, T. R.; Emori, S.; Kainuma, M.; Kram, T.; et al. The next Generation of Scenarios for  
38 Climate Change Research and Assessment. *Nature* **2010**, *463* (7282), 747–756.  
39 (2) Ragauskas, A. J.; Williams, C. K.; Davison, B. H.; Britovsek, G.; Cairney, J.; Eckert, C. A.;  
40 Frederick, W. J.; Hallett, J. P.; Leak, D. J.; Liotta, C. L.; et al. The Path Forward for Biofuels and  
41 Biomaterials. *Science* **2006**, *311* (5760), 484–489.  
42 (3) Bridgwater, A. V. Renewable Fuels and Chemicals by Thermal Processing of Biomass. *Chem.*  
43 *Eng. J.* **2003**, *91* (2–3), 87–102.  
44 (4) Vamvuka, D. Bio-Oil, Solid and Gaseous Biofuels from Biomass Pyrolysis Processes—An  
45 Overview. *Int. J. Energy Res.* **2011**, *35* (10), 835–862.  
46 (5) Lédé, J.; Broust, F.; Ndiaye, F.-T.; Ferrer, M. Properties of Bio-Oils Produced by Biomass Fast  
47 Pyrolysis in a Cyclone Reactor. *Fuel* **2007**, *86* (12–13), 1800–1810.  
48 (6) Diebold, J. P. *A Review of the Chemical and Physical Mechanisms of the Storage Stability of*  
49 *Fast Pyrolysis Bio-Oils*; Golden CO: National Renewable Energy Laboratory; 2000.  
50 (7) Czernik, S.; Bridgwater, A. V. Overview of Applications of Biomass Fast Pyrolysis Oil. *Energy*  
51 *Fuels* **2004**, *18* (2), 590–598.  
52 (8) Huber, G. W.; Iborra, S.; Corma, A. Synthesis of Transportation Fuels from Biomass:  
53 Chemistry, Catalysts, and Engineering. *Chem. Rev.* **2006**, *106* (9), 4044–4098.  
54 (9) Mortensen, P. M.; Grunwaldt, J.-D.; Jensen, P. A.; Knudsen, K. G.; Jensen, A. D. A Review of  
55 Catalytic Upgrading of Bio-Oil to Engine Fuels. *Appl. Catal. Gen.* **2011**, *407* (1–2), 1–19.  
56  
57  
58  
59  
60

- 1  
2  
3 (10) Liu, C.; Wang, H.; Karim, A. M.; Sun, J.; Wang, Y. Catalytic Fast Pyrolysis of Lignocellulosic  
4 Biomass. *Chem. Soc. Rev.* **2014**, *43* (22), 7594–7623.
- 5 (11) Kanaujia, P. K.; Sharma, Y. K.; Garg, M. O.; Tripathi, D.; Singh, R. Review of Analytical Strategies  
6 in the Production and Upgrading of Bio-Oils Derived from Lignocellulosic Biomass. *J. Anal.*  
7 *Appl. Pyrolysis* **2014**, *105*, 55–74.
- 8 (12) Jacobson, K.; Maheria, K. C.; Kumar Dalai, A. Bio-Oil Valorization: A Review. *Renew. Sustain.*  
9 *Energy Rev.* **2013**, *23*, 91–106.
- 10 (13) Mante, O. D.; Agblevor, F. A. Catalytic Pyrolysis for the Production of Refinery-Ready Biocrude  
11 Oils from Six Different Biomass Sources. *Green Chem.* **2014**, *16* (6), 3364–3377.
- 12 (14) Demirbas, A. Combustion of Biomass. *Energy Sources Part -Recovery Util. Environ. Eff.* **2007**,  
13 *29* (6), 549–561.
- 14 (15) Puertolas, B.; Veses, A.; Soledad Callen, M.; Mitchell, S.; Garcia, T.; Perez-Ramirez, J. Porosity-  
15 Acidity Interplay in Hierarchical ZSM-5 Zeolites for Pyrolysis Oil Valorization to Aromatics.  
16 *Chemsuschem* **2015**, *8* (19), 3283–3293.
- 17 (16) García, T.; Veses, A.; López, J. M.; Puértolas, B.; Pérez-Ramírez, J.; Callén, M. S. Determining  
18 Bio-Oil Composition via Chemometric Tools Based on Infrared Spectroscopy. *ACS Sustain.*  
19 *Chem. Eng.* **2017**, *5* (10), 8710–8719.
- 20 (17) Pattiya, A.; Titiloye, J. O.; Bridgwater, A. V. Fast Pyrolysis of Cassava Rhizome in the Presence  
21 of Catalysts. *J. Anal. Appl. Pyrolysis* **2008**, *81* (1), 72–79.
- 22 (18) Stefanidis, S.; Kalogiannis, K.; Iliopoulou, E. F.; Lappas, A. A.; Triguero, J. M.; Navarro, M. T.;  
23 Chica, A.; Rey, F. Mesopore-Modified Mordenites as Catalysts for Catalytic Pyrolysis of  
24 Biomass and Cracking of Vacuum Gasoil Processes. *Green Chem.* **2013**, *15* (6), 1647–1658.
- 25 (19) Cole, D. P.; Lee, Y. J. Effective Evaluation of Catalytic Deoxygenation for in Situ Catalytic Fast  
26 Pyrolysis Using Gas Chromatography–high Resolution Mass Spectrometry. *J. Anal. Appl.*  
27 *Pyrolysis* **2015**, *112*, 129–134.
- 28 (20) Bi, Y.; Wang, G.; Shi, Q.; Xu, C.; Gao, J. Compositional Changes during Hydrodeoxygenation of  
29 Biomass Pyrolysis Oil. *Energy Fuels* **2014**, *28* (4), 2571–2580.
- 30 (21) Koike, N.; Hosokai, S.; Takagaki, A.; Nishimura, S.; Kikuchi, R.; Ebitani, K.; Suzuki, Y.; Oyama, S.  
31 T. Upgrading of Pyrolysis Bio-Oil Using Nickel Phosphide Catalysts. *J. Catal.* **2016**, *333*, 115–  
32 126.
- 33 (22) Tessarolo, N. S.; Silva, R. V. S.; Vanini, G.; Casilli, A.; Ximenes, V. L.; Mendes, F. L.; de Rezende  
34 Pinho, A.; Romão, W.; de Castro, E. V. R.; Kaiser, C. R.; et al. Characterization of Thermal and  
35 Catalytic Pyrolysis Bio-Oils by High-Resolution Techniques: 1H NMR, GC × GC-TOFMS and FT-  
36 ICR MS. *J. Anal. Appl. Pyrolysis* **2016**, *117*, 257–267.
- 37 (23) Olcese, R.; Carré, V.; Aubriet, F.; Dufour, A. Selectivity of Bio-Oils Catalytic Hydrotreatment  
38 Assessed by Petroleomic and GC\*GC/MS-FID Analysis. *Energy Fuels* **2013**, *27* (4), 2135–2145.
- 39 (24) Stas, M.; Chudoba, J.; Auersvald, M.; Kubicka, D.; Conrad, S.; Schulzke, T.; Pospisil, M.  
40 Application of Orbitrap Mass Spectrometry for Analysis of Model Bio-Oil Compounds and Fast  
41 Pyrolysis Bio-Oils from Different Biomass Sources. *J. Anal. Appl. Pyrolysis* **2017**, *124*, 230–238.
- 42 (25) Hertzog, J.; Carré, V.; Le Brech, Y.; Mackay, C. L.; Dufour, A.; Mašek, O.; Aubriet, F.  
43 Combination of Electrospray Ionization, Atmospheric Pressure Photoionization and Laser  
44 Desorption Ionization Fourier Transform Ion Cyclotron Resonance Mass Spectrometry for  
45 the Investigation of Complex Mixtures - Application to the Petroleomic Analysis of Bio-Oils.  
46 *Anal. Chim. Acta* **2017**, *969*, 26–34.
- 47 (26) Jia, L.; Le-Brech, Y.; Shrestha, B.; Bente-von Frowein, M.; Ehlert, S.; Mauviel, G.; Zimmermann,  
48 R.; Dufour, A. Fast Pyrolysis in a Microfluidized Bed Reactor: Effect of Biomass Properties and  
49 Operating Conditions on Volatiles Composition as Analyzed by Online Single Photoionization  
50 Mass Spectrometry. *Energy Fuels* **2015**, *29* (11), 7364–7374.
- 51 (27) Le Brech, Y.; Jia, L.; Cissé, S.; Mauviel, G.; Brosse, N.; Dufour, A. Mechanisms of Biomass  
52 Pyrolysis Studied by Combining a Fixed Bed Reactor with Advanced Gas Analysis. *J. Anal. Appl.*  
53 *Pyrolysis* **2016**, *117*, 334–346.
- 54 (28) Jia, L.; Buendia-Kandia, F.; Dumarcay, S.; Poirot, H.; Mauviel, G.; Gerardin, P.; Dufour, A. Fast  
55 Pyrolysis of Heartwood, Sapwood, and Bark: A Complementary Application of Online  
56  
57  
58  
59  
60

- 1  
2  
3 Photoionization Mass Spectrometry and Conventional Pyrolysis Gas Chromatography/Mass  
4 Spectrometry. *Energy Fuels* **2017**, *31* (4), 4078–4089.
- 5 (29) Jia, L.; Raad, M.; Hamieh, S.; Toufaily, J.; Hamieh, T.; Bettahar, M.; Mauviel, G.; Tarrighi, M.;  
6 Pinard, L.; Dufour, A. Catalytic Fast Pyrolysis of Biomass: Superior Selectivity of Hierarchical  
7 Zeolite to Aromatics. *Green Chem.* **2017**.
- 8 (30) Jia, L.; Dufour, A.; Le Brech, Y.; Authier, O.; Mauviel, G. On-Line Analysis of Primary Tars from  
9 Biomass Pyrolysis by Single Photoionization Mass Spectrometry: Experiments and Detailed  
10 Modelling. *Chem. Eng. J.* **2017**, *313*, 270–282.
- 11 (31) Wang, X.; Kersten, S. R. A.; Prins, W.; van Swaaij, W. P. M. Biomass Pyrolysis in a Fluidized Bed  
12 Reactor. Part 2: Experimental Validation of Model Results. *Ind. Eng. Chem. Res.* **2005**, *44* (23),  
13 8786–8795.
- 14 (32) Venderbosch, R. H.; Prins, W. Fast Pyrolysis Technology Development. *Biofuels Bioprod.*  
15 *Biorefining-Biofpr* **2010**, *4* (2), 178–208.
- 16 (33) Verboekend, D.; Perez-Ramirez, J. Design of Hierarchical Zeolite Catalysts by Desilication.  
17 *Catal. Sci. Technol.* **2011**, *1* (6), 879–890.
- 18 (34) Hertzog, J.; Carré, V.; Le Brech, Y.; Dufour, A.; Aubriet, F. Toward Controlled Ionization  
19 Conditions for ESI-FT-ICR-MS Analysis of Bio-Oils from Lignocellulosic Material. *Energy Fuels*  
20 **2016**, *30* (7), 5729–5739.
- 21 (35) Miettinen, I.; Kuitinen, S.; Paasikallio, V.; Mäkinen, M.; Pappinen, A.; Jänis, J. Characterization  
22 of Fast Pyrolysis Oil from Short-Rotation Willow by High-Resolution Fourier Transform Ion  
23 Cyclotron Resonance Mass Spectrometry. *Fuel* **2017**, *207* (Supplement C), 189–197.
- 24 (36) Staš, M.; Chudoba, J.; Kubicka, D.; Blazek, J.; Pospíšil, M. Petroleomic Characterization of  
25 Pyrolysis Bio-Oils: A Review. *Energy Fuels* **2017**.
- 26 (37) Pudenzi, M. A.; Eberlin, M. N. Assessing Relative Electrospray Ionization, Atmospheric  
27 Pressure Photoionization, Atmospheric Pressure Chemical Ionization, and Atmospheric  
28 Pressure Photo- and Chemical Ionization Efficiencies in Mass Spectrometry Petroleomic  
29 Analysis via Pools and Pairs of Selected Polar Compound Standards. *Energy Fuels* **2016**, *30* (9),  
30 7125–7133.
- 31 (38) Bi, Z.; Zhang, J.; Peterson, E.; Zhu, Z.; Xia, C.; Liang, Y.; Wiltowski, T. Biocrude from Pretreated  
32 Sorghum Bagasse through Catalytic Hydrothermal Liquefaction. *Fuel* **2017**, *188*, 112–120.
- 33 (39) Cheng, Y.-T.; Huber, G. W. Production of Targeted Aromatics by Using Diels-Alder Classes of  
34 Reactions with Furans and Olefins over ZSM-5. *Green Chem.* **2012**, *14* (11), 3114–3125.
- 35 (40) Veses, A.; Puertolas, B.; Manuel Lopez, J.; Soledad Callen, M.; Solsona, B.; Garcia, T. Promoting  
36 Deoxygenation of Bio-Oil by Metal-Loaded Hierarchical ZSM-5 Zeolites. *ACS Sustain. Chem.*  
37 *Eng.* **2016**, *4* (3), 1653–1660.
- 38 (41) Gayubo, A. G.; Valle, B.; Aguayo, A. T.; Olazar, M.; Bilbao, J. Attenuation of Catalyst  
39 Deactivation by Cofeeding Methanol for Enhancing the Valorisation of Crude Bio-Oil. *Energy*  
40 *Fuels* **2009**, *23* (8), 4129–4136.
- 41 (42) Hoff, T. C.; Holmes, M. J.; Proano-Aviles, J.; Emdadi, L.; Liu, D.; Brown, R. C.; Tessonier, J.-P.  
42 Decoupling the Role of External Mass Transfer and Intracrystalline Pore Diffusion on the  
43 Selectivity of HZSM-5 for the Catalytic Fast Pyrolysis of Biomass. *ACS Sustain. Chem. Eng.* **2017**,  
44 *5* (10), 8766–8776.
- 45 (43) Pinard, L.; Hamieh, S.; Canaff, C.; Ferreira Madeira, F.; Batonneau-Gener, I.; Maury, S.;  
46 Delpoux, O.; Ben Tayeb, K.; Pouilloux, Y.; Vezin, H. Growth Mechanism of Coke on HBEA  
47 Zeolite during Ethanol Transformation. *J. Catal.* **2013**, *299*, 284–297.
- 48 (44) Kim, J.; Choi, M.; Ryoo, R. Effect of Mesoporosity against the Deactivation of MFI Zeolite  
49 Catalyst during the Methanol-to-Hydrocarbon Conversion Process. *J. Catal.* **2010**, *269* (1),  
50 219–228.  
51  
52  
53  
54

## 55 CAPTION

56  
57  
58  
59  
60

1  
2  
3 **Table 1:** Relative distribution of compound families identified in positive and negative ion ESI, LDI,  
4 and APPI FT-ICR MS in raw bio-oil and upgraded A and B bio-oils from the pyrolysis of the 1-  
5 7 and 8-14 oak cylinders.  
6

7  
8 **Figure 1:** Relative distribution of  $C_xH_y$  and  $C_xH_yO_z$  compounds in respect with the number of oxygen  
9 atoms in positive and negative ion ESI, LDI, and APPI FT-ICR MS for raw bio-oil and upgraded  
10 A and B bio-oils from the pyrolysis of the 1-7 and 8-14 oak cylinders.  
11

12  
13 **Figure 2:** Relative intensities of the  $C_xH_y$  and  $C_xH_yO_z$  compounds in raw bio-oil and upgraded A and B  
14 bio-oils from the pyrolysis of the 1-7 oak cylinders represented on the van Krevelen  
15 diagrams according to their H/C and O/C ratios as obtained by (+) and (-) ESI, APPI, and LDI  
16 FT-ICR MS.  
17

18  
19  
20 **Figure 3:** Carbon number vs. DBE distribution of  $C_xH_y$  compounds observed in (+) APPI and (-) LDI for  
21 raw bio-oil and upgraded A and B bio-oils from the pyrolysis of the 1-7 (top) and 8-14  
22 (bottom) oak cylinders.  
23

24  
25 **Figure 4:** Carbon number vs. DBE distribution of  $C_xH_yO_z$  compounds observed in (+) APPI for raw bio-  
26 oil and upgraded A and B bio-oils from the pyrolysis of the 1-7 oak cylinders.  
27

28  
29 **Figure 5:** Relative intensities of the  $C_xH_y$  and  $C_xH_yO_z$  compounds in raw bio-oil and upgraded A and B  
30 bio-oils from the pyrolysis of the 8-14 oak cylinders represented on the van Krevelen  
31 diagrams according to their H/C and O/C ratios as obtained by (+) and (-) ESI, APPI, and LDI  
32 FT-ICR MS  
33  
34  
35  
36  
37  
38  
39  
40  
41  
42  
43  
44  
45  
46  
47  
48  
49  
50  
51  
52  
53  
54  
55  
56  
57  
58  
59  
60



Table 1

	SAMPLES	# <sup>12</sup> C SIGNALS	C <sub>x</sub> H <sub>y</sub>	C <sub>x</sub> H <sub>y</sub> O <sub>z</sub>	C <sub>x</sub> H <sub>y</sub> N <sub>n</sub> O <sub>z</sub>	C <sub>x</sub> H <sub>y</sub> SO <sub>z</sub>
<b>(+) ESI</b>	Raw BO	1577	-	92 %	8 %	-
	BO A 1-7	629	-	90 %	10 %	-
	BO A 8-14	1298	-	89 %	11 %	-
	BO B 1-7	496	-	96 %	4 %	-
	BO B 8-14	487	-	96 %	4 %	-
<b>(-) ESI</b>	Raw BO	1290	-	92 %	1 %	7 %
	BO A 1-7	1890	-	91 %	2 %	7 %
	BO A 8-14	1516	-	91 %	2 %	7 %
	BO B 1-7	1944	-	88 %	3 %	9 %
	BO B 8-14	1778	-	91 %	2 %	7 %
<b>(+) APPI</b>	Raw BO	1662	1 %	98 %	1 %	-
	BO A 1-7	2141	2 %	98 %	-	-
	BO A 8-14	2185	1 %	99 %	< 1 %	-
	BO B 1-7	1361	14 %	85 %	< 1 %	-
	BO B 8-14	1276	3 %	97 %	-	-
<b>(-) LDI</b>	Raw BO	510	< 1 %	91 %	-	9 %
	BO A 1-7	436	5 %	91 %	-	4 %
	BO A 8-14	1203	-	99 %	-	1 %
	BO B 1-7	944	6 %	93 %	-	1 %
	BO B 8-14	1142	-	91 %	-	9 %

Figure 1

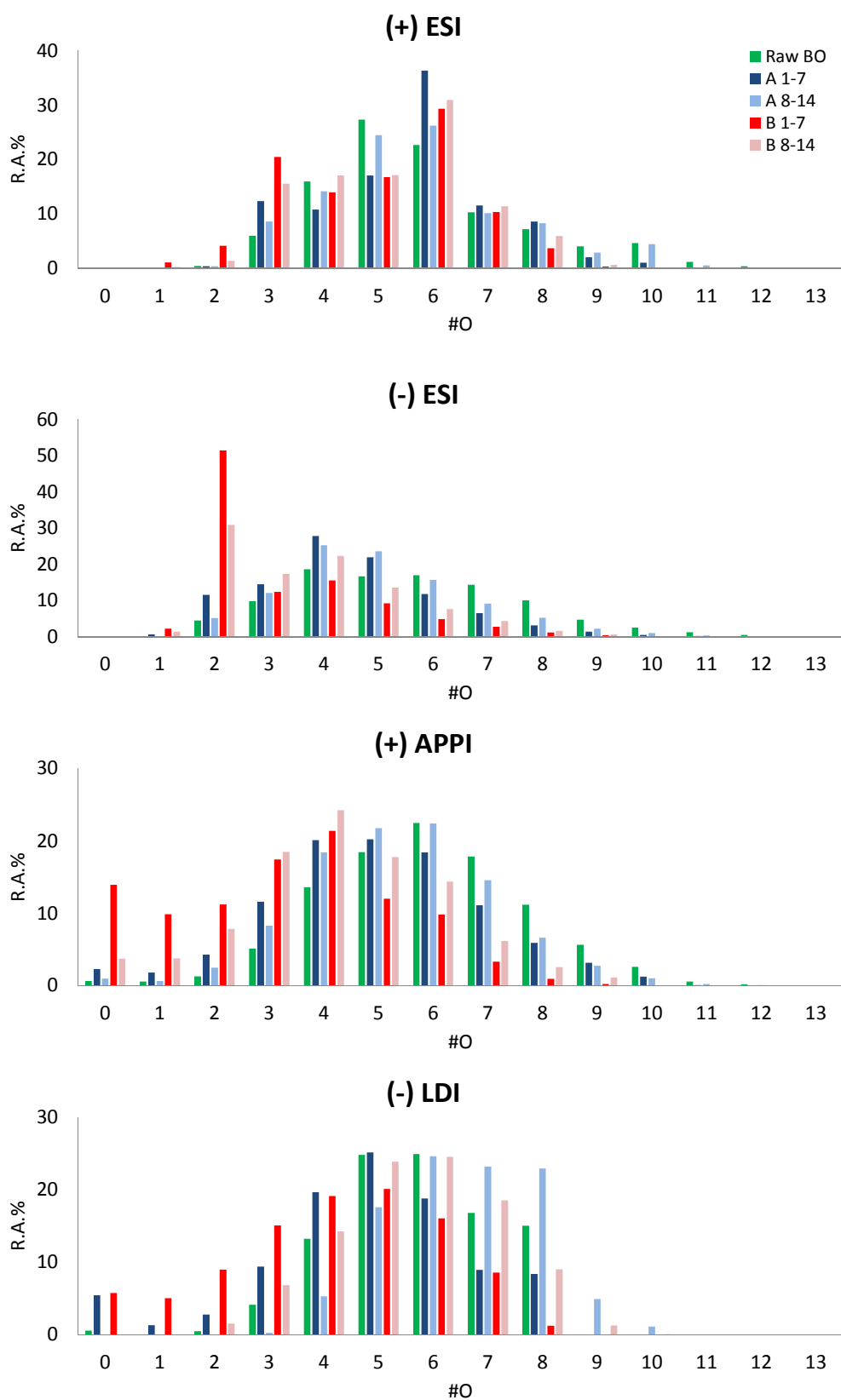


Figure 2

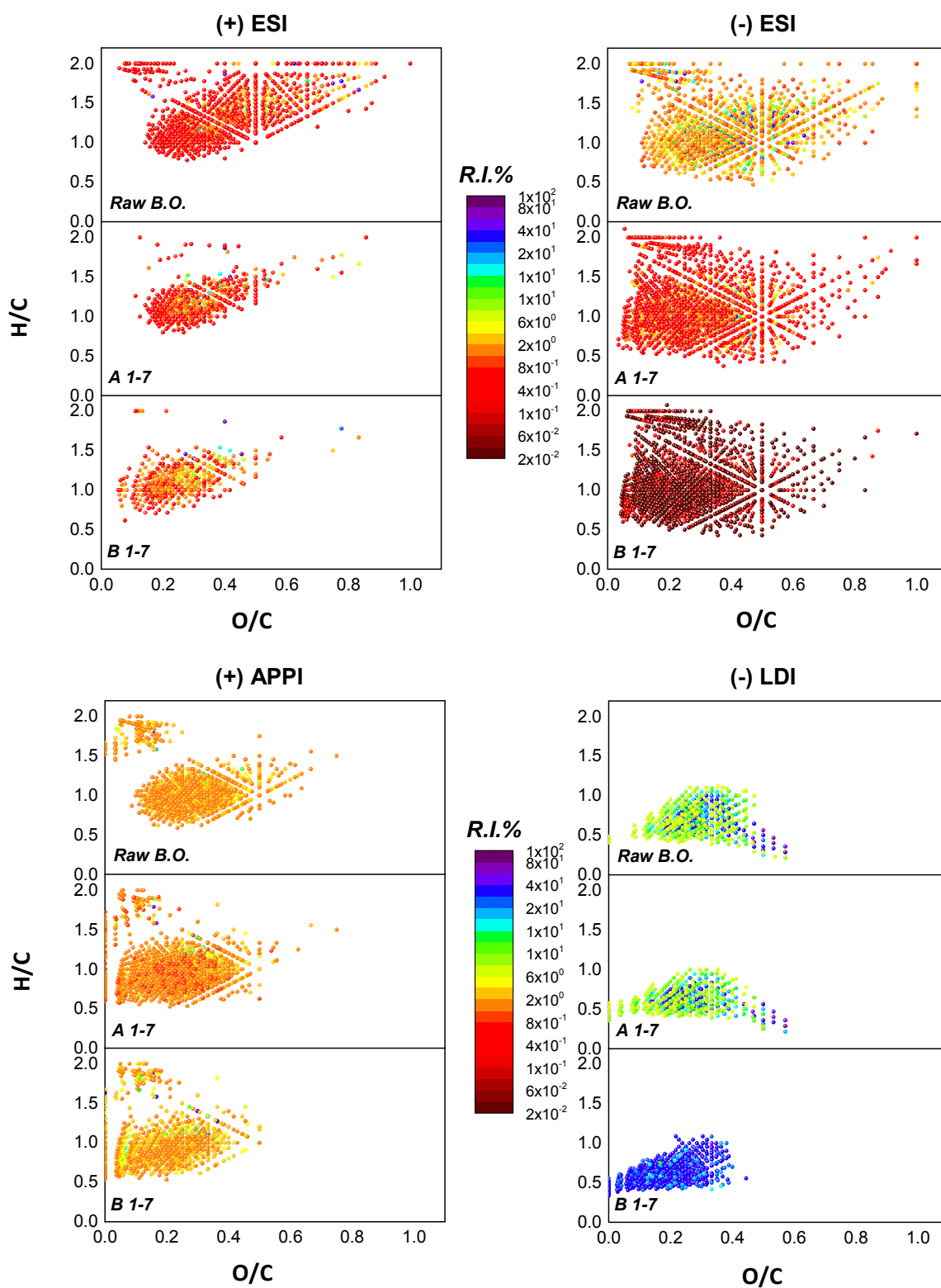


Figure 3

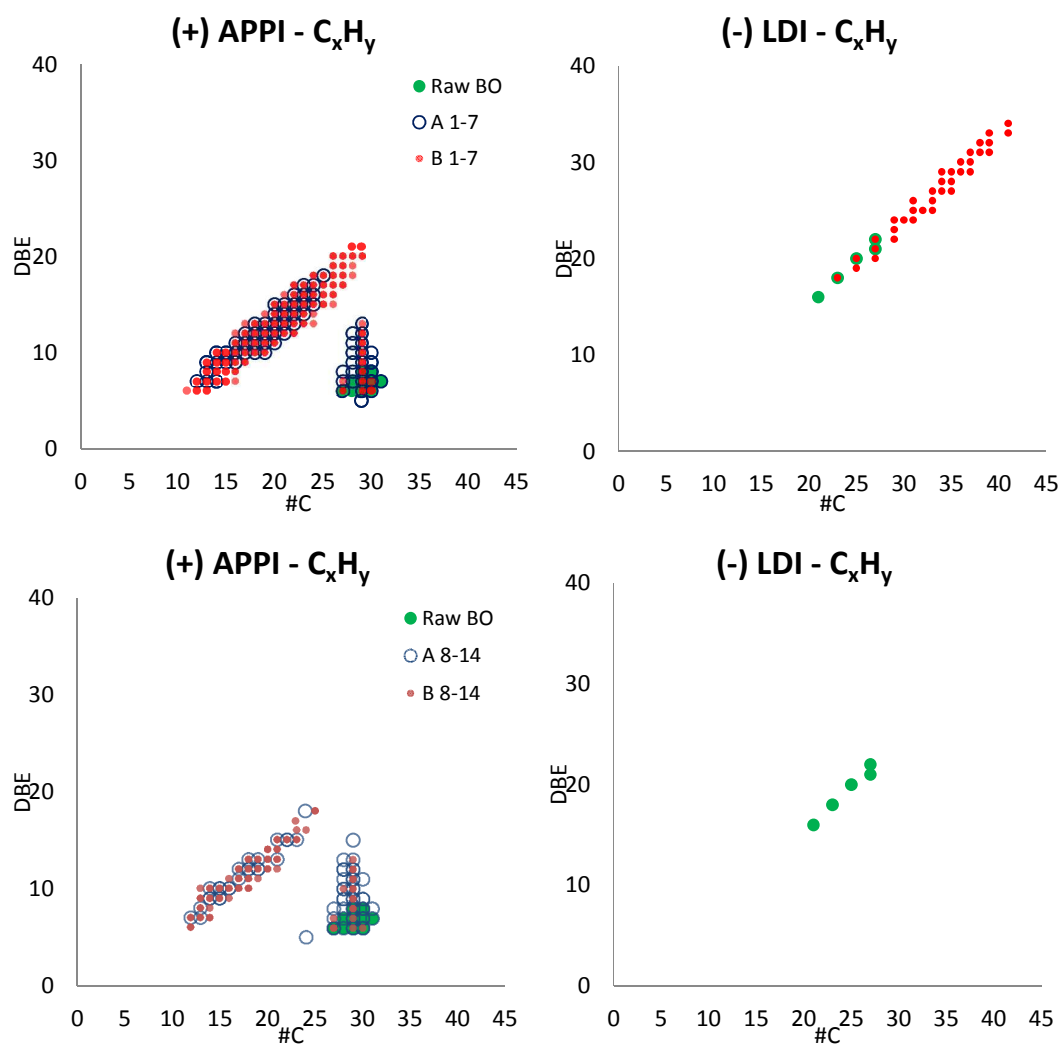


Figure 4

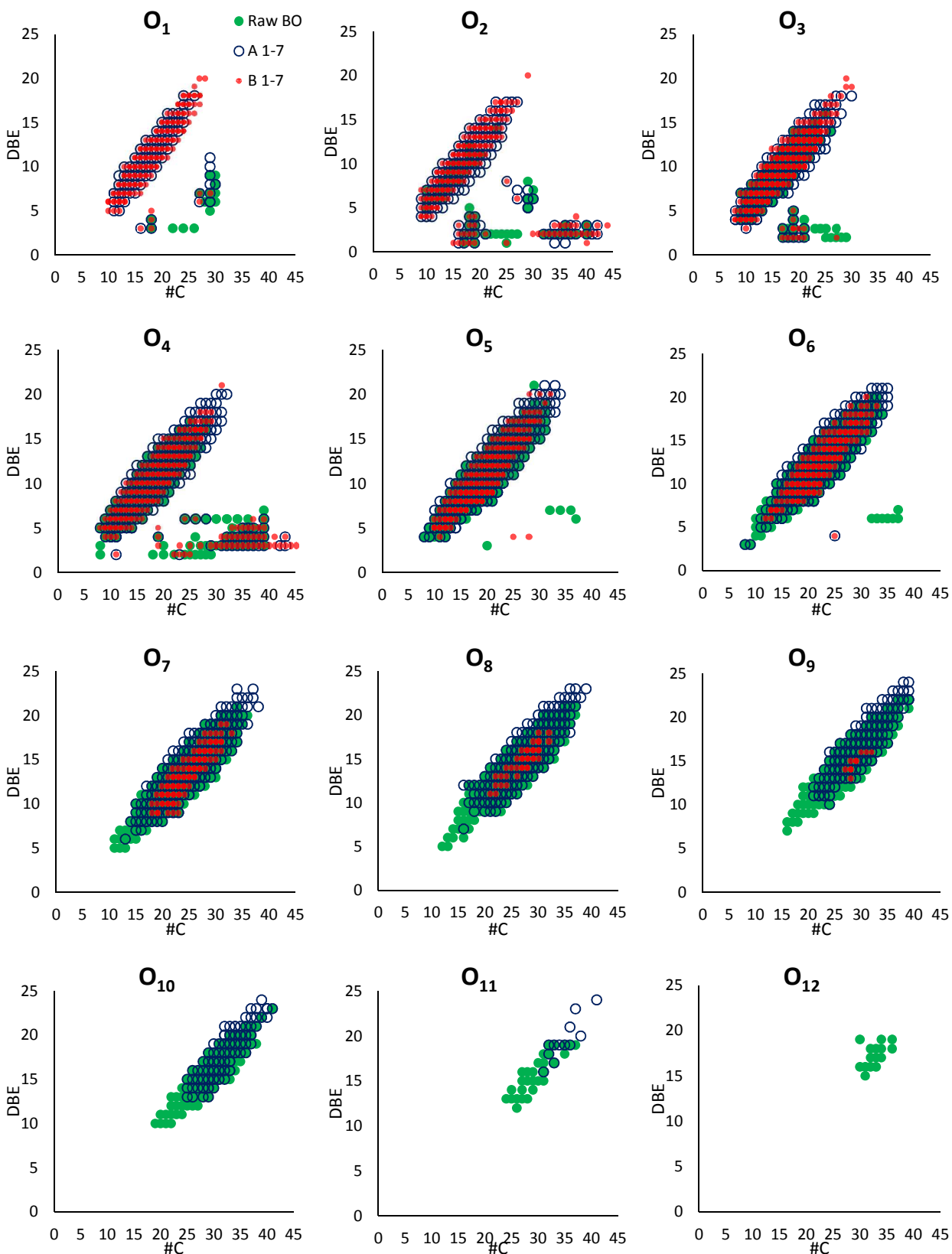
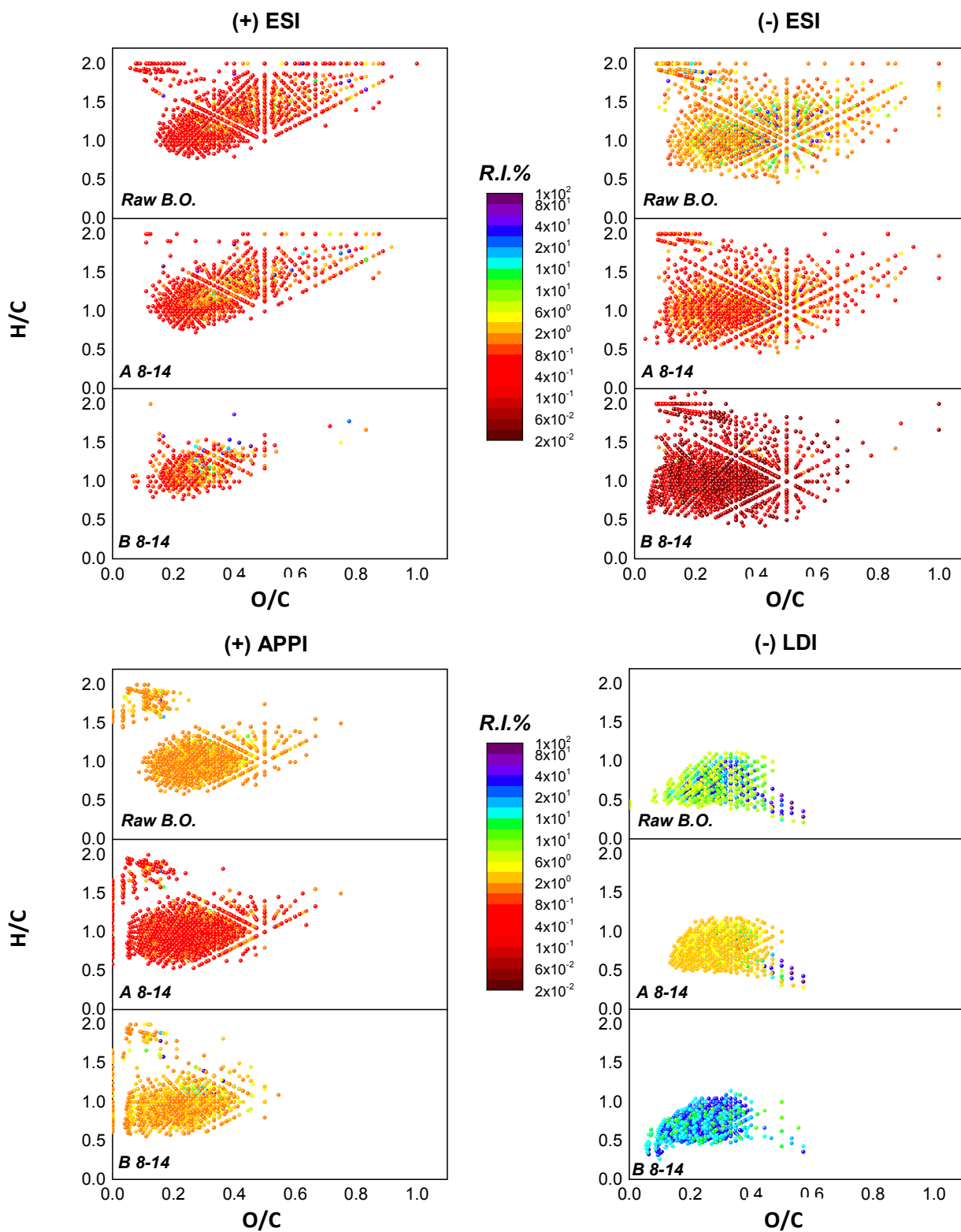


Figure 5



1  
2  
3  
4  
5  
6  
7  
8  
9  
10  
11  
12  
13  
14  
15  
16  
17  
18  
19  
20  
21  
22  
23  
24  
25  
26  
27  
28  
29  
30  
31  
32  
33  
34  
35  
36  
37  
38  
39  
40  
41  
42  
43  
44  
45  
46  
47  
48  
49  
50  
51  
52  
53  
54  
55  
56